

See discussions, stats, and author profiles for this publication at: <https://www.researchgate.net/publication/50373474>

Wetting and Spreading of Nanofluids on Solid Surfaces Driven by the Structural Disjoining Pressure: Statics Analysis and Experiments

ARTICLE in LANGMUIR · MARCH 2011

Impact Factor: 4.46 · DOI: 10.1021/la104204b · Source: PubMed

CITATIONS

28

READS

108

4 AUTHORS:



Kirti Kondiparty

Ecolab

3 PUBLICATIONS 99 CITATIONS

[SEE PROFILE](#)



Alex Nikolov

Illinois Institute of Technology

148 PUBLICATIONS 3,153 CITATIONS

[SEE PROFILE](#)



Stanley Wu

Illinois Institute of Technology

12 PUBLICATIONS 86 CITATIONS

[SEE PROFILE](#)



D. T. Wasan

Illinois Institute of Technology

354 PUBLICATIONS 7,668 CITATIONS

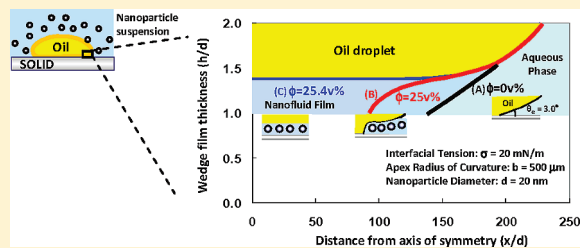
[SEE PROFILE](#)

Wetting and Spreading of Nanofluids on Solid Surfaces Driven by the Structural Disjoining Pressure: Statics Analysis and Experiments

Kirti Kondiparty, Alex Nikolov, Stanley Wu, and Darsh Wasan*

Department of Chemical and Biological Engineering, Illinois Institute of Technology, Chicago, Illinois 60616, United States

ABSTRACT: The wetting and spreading of nanofluids composed of liquid suspensions of nanoparticles have significant technological applications. Recent studies have revealed that, compared to the spreading of base liquids without nanoparticles, the spreading of wetting nanofluids on solid surfaces is enhanced by the structural disjoining pressure. Here, we present our experimental observations and the results of the statics analysis based on the augmented Laplace equation (which takes into account the contribution of the structural disjoining pressure) on the effects of the nanoparticle concentration, nanoparticle size, contact angle, and drop size (i.e., the capillary and hydrostatic pressure); we examined the effects on the displacement of the drop-meniscus profile and spontaneous spreading of a nanofluid as a film on a solid surface. Our analyses indicate that a suitable combination of the nanoparticle concentration, nanoparticle size, contact angle, and capillary pressure can result not only in the displacement of the three-phase contact line but also in the spontaneous spreading of the nanofluid as a film on a solid surface. We show here, for the first time, that the complete wetting and spontaneous spreading of the nanofluid as a film driven by the structural disjoining pressure gradient (arising due to the nanoparticle ordering in the confined wedge film) is possible by decreasing the nanoparticle size and the interfacial tension, even at a nonzero equilibrium contact angle. Experiments were conducted on the spreading of a nanofluid composed of 5, 10, 12.5, and 20 vol % silica suspensions of 20 nm (geometric diameter) particles. A drop of canola oil was placed underneath the glass surface surrounded by the nanofluid, and the spreading of the nanofluid was monitored using an advanced optical technique. The effect of an electrolyte, such as sodium chloride, on the nanofluid spreading phenomena was also explored. On the basis of the experimental results, we can conclude that a nanofluid with an effective particle size (including the electrical double layer) of about 40 nm, a low equilibrium contact angle ($<3^\circ$), and a high effective volume concentration (>30 vol %) is desirable for the dynamic spreading of a nanofluid system with an interfacial tension of 0.5 mN/m. Our experimental observations also validate the major predictions of our theoretical analysis.



INTRODUCTION

The wetting and spreading of nanofluid films with self-organized structures, such as suspensions of nanosized particles, polymer latexes, globular proteins, and surfactant micelles (or microemulsions), have significant technological applications in nanotechnology and biological systems.¹ For example, their spreading and adhesion behavior on solid surfaces can yield materials with desirable structural and optical properties.²

Recent experiments conducted in our laboratory have clearly demonstrated that the spreading and wetting of nanofluids on solids (i.e., nanoparticle dispersions in liquids) are enhanced due to the nanoparticle self-structuring in the confined three-phase oil-nanofluid–solid contact region that is inside the wedge film between an oil drop and a solid surface (Figure 2a,b). Nanoparticles inside the wedge film tend to form more ordered structures (due to the collective interactions) in the confined region than those in the bulk meniscus.^{3–14} This structuring is a consequence of the fact that the ordering increases the entropy of the overall dispersion by permitting greater freedom for the nanoparticles in the bulk liquid. The result is that these ordered microstructures exert excess pressure (i.e., the disjoining pressure) in a film

relative to that in the bulk solution, separating the two surfaces confining the nanofluid. Theoretical calculations based on the statistical mechanics approach and Monte Carlo simulations have indicated that the particles are highly structured close to the vertex and become more randomly packed as the radial distance increases toward the bulk solution. The film structural disjoining pressure (i.e., the osmotic component in the excess pressure) in the wedge film exerted by the particles normal to the confining surfaces is high near the vertex. It has an oscillatory decay with the increasing film thickness, and both the period of oscillation and decay factor are equal to the average diameter (including the double layer) surrounding the nanoparticle^{15–17} (Figure 1).

Recently, Nikolov et al.,¹⁸ using the combined differential and common reflected light interference methods,^{19–21} investigated the film-meniscus profile of an oil drop on a smooth, horizontal hydrophilic glass surface in the presence of an aqueous

Received: October 19, 2010

Revised: December 29, 2010

Published: March 11, 2011

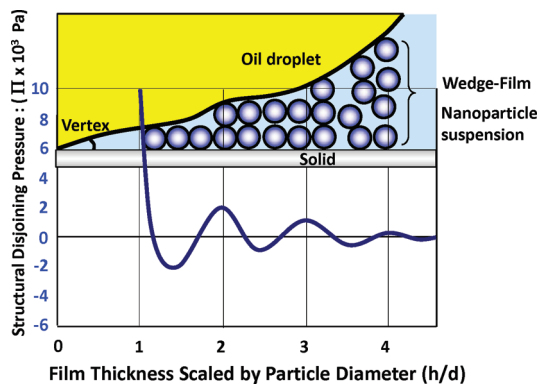


Figure 1. Pressure on the walls of wedge for 0.5° contact angle at the vertex as a function of radial distance. Particle volume fraction $\phi = 0.36$ and particle diameter $d = 10 \text{ nm}$.⁴

suspension of silica nanoparticles. Experiments revealed that the fluid wedge deformed under the action of the structural film disjoining pressure (Figure 2a,b).¹⁹

The classical concepts of simple liquid wetting and spreading do not apply to nano- and complex fluids.^{22–28} The complex nature of the interactions between the particles in the nanofluid and with the solid substrate greatly alters the spreading dynamics under the action of the disjoining pressure gradient.^{28–34}

The spreading of pure fluids is generally described in terms of the spreading coefficient S , given by

$$S = \sigma_{s/o} - \sigma_{s/l} - \sigma_{o/l} \quad (1)$$

where σ is the respective interfacial tension existing between the solid–oil ($\sigma_{s/o}$), solid–nanofluid ($\sigma_{s/l}$), and the oil–nanofluid phase ($\sigma_{o/l}$). When we combine eq 1 with the Gibbs equation for the equilibrium contact angle, we get

$$S = \sigma_{s/o} - \sigma_{s/l} - \sigma_{o/l} = \sigma_{o/l}(\cos \theta_e - 1) \quad (2)$$

where θ_e is the equilibrium contact angle. Therefore, according to the classical theory of wetting and spreading, pure liquids (without any nanoparticles) spontaneously spread or wet the surface only when the equilibrium contact angle is zero. However, nanofluid spreading or wetting is enhanced by the structural disjoining pressure because of the ordering of the nanoparticles confined in the wedge film.

The contact angle, θ_e , of the wedge film is related to the disjoining pressure, given by the Frumkin–Derjaguin equation:^{36–44,57,58}

$$S = \Pi_0(h_e)h_e + \int_{h_e}^{\infty} \Pi(h) dh = \sigma_{o/l}(\cos \theta_e - 1) \quad (3)$$

here h_e is the equilibrium thickness of a thick film, Π_0 is represented by the sum of the capillary pressure, P_c , and hydrostatic pressure, P_g , of the droplet, and Π is the disjoining pressure, represented by three major terms: $\Pi = \Pi_{vw} + \Pi_d + \Pi_{st}$. Π_{vw} represents the pressure arising from the short-range van der Waals force, Π_d accounts for the pressure arising from forces that are electrostatic or stearic in nature and Π_{st} represents the pressure due to long-range structural forces arising from the ordering of the nanofluid's particles in the wedge film (Figures 1 and 2). The second term on the right side of eq 3, which is the integral of the disjoining pressure, is the film tension (i.e., the film

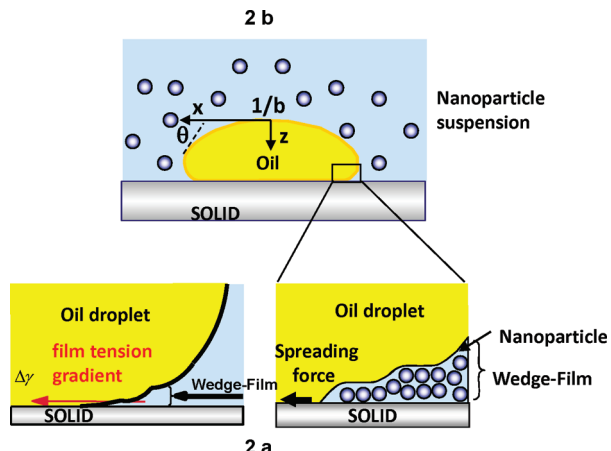


Figure 2. Nanoparticle structuring in the wedge-film resulting in structural disjoining pressure gradient/film tension gradient at the wedge vertex.

energy). The contact angle, θ_e , in the last term of eq 3 is the equilibrium microscopic contact angle between the film and the meniscus. The film tension gradient is directed toward the wedge film from the bulk solution and is high near the vertex because of the nanoparticle structuring in the wedge confinement. As the film tension increases toward the vertex of the wedge, it drives the nanofluid to spread out at the wedge tip (the three-phase contact line moves), thereby enhancing the dynamic spreading of the nanofluid (Figure 2a,b). When the film tension gradient is higher than the bulk-meniscus capillary pressure, the nanofluid spontaneously spreads on the solid surface (i.e., $S \geq 0$), even at $\theta_e \geq 0$.

The effects of various components of the disjoining pressure (e.g., van der Waals, electrostatic, and solvation forces) on spreading, wetting, and the position of the three-phase contact line, have been studied previously.^{50–56,59} Our prior calculations for the spreading behavior of partially wetting nanofluids using the augmented Laplace equation (which takes into account the contribution of the structural disjoining pressure) showed that the structural disjoining pressure arising from the structuring of the nanoparticles in the liquid film results in the displacement of the three-phase contact line.^{10,30}

In the present study, we systematically investigated (theoretically and experimentally) the effects of the nanoparticle concentration, particle size, contact angle, interfacial tension, and the total pressure (i.e., including the contributions from the bulk-meniscus capillary pressure and the hydrostatic pressure of the drop) on the equilibrium film–meniscus profile and the movement of the contact line under the action of the structural disjoining pressure gradient. We carried out a statics (equilibrium) analysis to predict a suitable combination of drop size, nanofluid concentration, nanoparticle size, and contact angle that would result in the complete wetting and spontaneous spreading of the nanofluid as a film on the solid surface. We also performed experiments using an advanced optical technique to monitor the spreading of the nanofluid film between the oil drop and the solid surface, as well as to validate the predictions from our statics analysis.

STATICS ANALYSIS

Chengara et al.^{10,30} calculated the displacement of the three-phase contact line in the wedge region under the action of the

structural disjoining pressure gradient of the nanofluid on hydrophilic solid surfaces. The structural disjoining pressure is significant only up to 4–5 times the effective particle diameter from the solid surface.^{4–13,10,30} Therefore, for calculating the wedge-film profile close to the solid surface, they augmented the Laplace equation by an additional term related to the structural disjoining pressure:

$$\frac{-\sigma \left(\frac{d^2 h}{dx^2} \right)}{\left[1 + \left(\frac{dh}{dx} \right)^2 \right]^{3/2}} - \Pi_{st}(h) + \Delta \rho g h = P_w - P_o \quad (4)$$

where P refers to the bulk pressure far from the wedge-film region and the subscripts w and o refer to the water and oil phases, respectively. The first term in eq 4 is the capillary pressure, the second term is the structural disjoining pressure, and the third term is the gravitational contribution or hydrostatic pressure, P_g .

In the analysis of Chengara et al.,^{10,30} the oil drop is considered one-dimensional with only one radius of curvature. However, the oil drop is actually two-dimensional with two radii of curvature, as shown in Figure 2a. Thus, in the present analysis, we solve for the meniscus profile of a two-dimensional oil drop. We can write the Laplace equations as three first-order differential equations:

$$\frac{dx}{ds} = \cos \theta \quad (5)$$

$$\frac{dz}{ds} = \sin \theta \quad (6)$$

$$\frac{d \sin \theta}{dx} + \frac{\sin \theta}{x} = \frac{2}{b} + \frac{\Delta \rho g z}{\sigma} - \frac{\Pi_{st}(h)}{\sigma} \quad (7)$$

where b is the apex radius of curvature and $\Delta \rho = \rho_w - \rho_o$ (the difference in the density between the nanofluid and oil phase). σ is the nanofluid–oil interfacial tension. θ is the running contact angle and s is the arc length measured from the apex as the origin where the rectangular coordinates $x = z = 0$. $\Pi_{st}(h)$ is the structural disjoining pressure arising from the ordering of nanoparticles in the confined film-meniscus region.

Trokhymchuk et al.⁶ developed an analytical expression for the structural disjoining pressure (Π_{st}) based on a solution of the Ornstein–Zernike statistical mechanics equation:

$$\Pi_{st}(h) = \Pi_1 \cos(\omega h + \varphi_2) e^{-\kappa h} + \Pi_2 e^{-\delta(h-d)} \quad \text{for } h \geq d \quad (8)$$

$$\Pi_{st}(h) = -P \quad \text{for } 0 < h < d \quad (9)$$

where d is the diameter of the nanoparticle, and all other parameters ($\Pi_1, \omega, \varphi_2, \kappa$) in eq 8 are fitted as cubic polynomials in terms of the nanofluid volume fraction (ϕ)⁶ (e.g., $a_0 + a_1\phi + a_2\phi^2 + a_3\phi^3$, while the constants' coefficients a_0, a_1, a_2, a_3 vary for each parameter). $\phi = n_p \pi d^3 / 6$, where n_p is the number of particles per unit volume of the system/nanofluid. However (usually due to the charge on the nanoparticle surface), when the nanoparticles are dispersed in a continuous medium, they are surrounded by a double layer of thickness, Δ . The effective diameter of the nanoparticles would then be $d_e = d + 2\Delta$. The nanoparticles are assumed to act as effective hard sphere particles

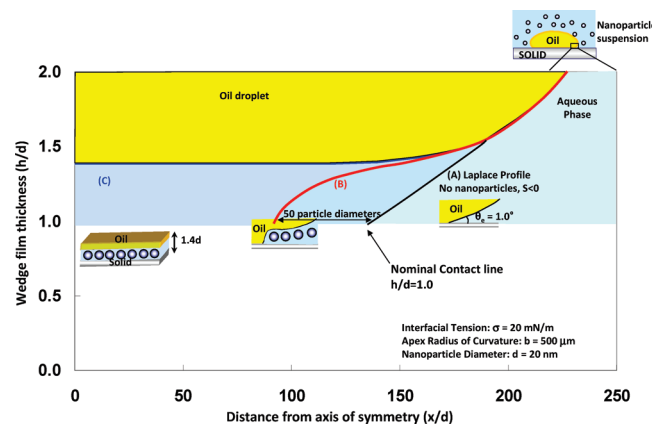


Figure 3. Effect of the structural disjoining pressure on the meniscus profile. (A) Meniscus profile in the absence of nanoparticles (Laplace equation). (B) Displacement of contact line due to nanoparticles ($S < 0$).¹⁰ $\phi = 25$ vol %. (C) Meniscus profile for complete spreading ($S = 0$). Nanofluid film. $\phi = 25.4$ vol %.

with diameters equal to d_e and the effective volume of the nanofluid is $\phi_e = n_p \pi d_e^3 / 6$.^{3,18} In eq 9, P refers to the bulk osmotic pressure of the nanofluid.

Equations 5–7 are solved subject to the boundary conditions on the running contact angle (θ) of the drop (Figure 2a), arc length (s), horizontal distance from the apex (x), and the vertical distance from the apex (z):

$$\theta = s = x = z = 0 \quad (10)$$

This equation defines the apex of the drop. We define the position of the nominal contact line as that radial distance at which the height of the meniscus becomes equal to the diameter of the nanoparticle: $z = d$. For a wedge-film thickness smaller than a nanoparticle diameter, the disjoining pressure is a combination of the depletion attraction between the film surfaces as well as the van der Waals contribution as determined from the Hamaker constant. Since our focus is on the contribution of the structural disjoining pressure from the nanoparticles to the nanofluid-spreading phenomenon, the region of the wedge-film thickness below a particle diameter was not considered. This simplification does not introduce a significant error, as noted by Chengara et al.¹⁰

Equations 5–7 are solved numerically using the Runge–Kutta–Verner fifth-order method. We calculated the meniscus profile for the base case first (when the disjoining pressure is zero) and the profile followed the classical Laplace equation. We then solved eqs 5–7 together with eq 8 for the meniscus profile in the presence of nanoparticles in the film-meniscus region. We calculated the meniscus profile starting from $z/d = 4$ and ended when the meniscus height equaled one particle diameter (i.e., $1 \leq z/d \leq 4$). This was because the meniscus profile beyond four particle diameters from the solid surface (i.e., $z/d > 4$) followed the classical Laplace equation, as the structural disjoining pressure was insignificant in this region.

RESULTS AND DISCUSSION

We solved eqs 5–8 for the wedge profile both in the presence and in the absence of nanoparticles. Figure 3 shows the wedge profiles for an oil drop (with an apex radius of curvature of 500 μm and 0.53 μL in volume) on a smooth solid surface with an

equilibrium three-phase contact angle of 1° (measured from the aqueous phase) and an oil–aqueous phase interfacial tension of 20 mN/m , corresponding to a hexadecane–water system. The aqueous nanofluid contains particles 20 nm in diameter. The effect of the nanoparticles on the displacement of the nominal contact line is clearly seen when we compare curves A and B. Curve A corresponds to a structural disjoining pressure of zero and the profile is given by the classical Laplace equation. There is a displacement of the nominal contact line by 50 particle diameters for a nanofluid with 25 vol\% of nanoparticles, 20 nm in diameter (curve B). The shape of the equilibrium wedge profiles is identical (in both the presence and absence of nanoparticles) to that calculated by Chengara et al.,¹⁰ we used the analytical solution from eq 2. This validates the model and accuracy of the numerical method used in our present analysis. It is evident that, due to the structural disjoining pressure arising from the nanoparticle ordering in the wedge film (Figure 1), the local slope of the profile (Figure 3, curve B) increases at the location where the height of the film is equal to the diameter of the nanoparticle.

When we increased the volume concentration of the nanoparticles from 25 to 25.4 vol\% , we found that the wedge profile further deformed and became parallel to the solid surface (Figure 3, curve C). The profile did not reach the solid surface, and the oil drop was now separated by a thin equilibrium film of fluid containing one layer of nanoparticles. The running contact angle at the axis of symmetry was zero, so the spreading coefficient as defined by eq 3 was zero ($S = 0$). The equilibrium contact angle (θ_e) was finite (1° in this case) and yet the nanofluid spread spontaneously as a film on the solid surface. Upon a further increase in the volume concentration of the nanofluid (above 25.4 vol\%), the profile retracted upward into the oil phase; this is not practically possible. Physically, at above 25.4 vol\% , the magnitude of the structural disjoining pressure becomes much larger than the sum of the capillary and hydrostatic pressures, so the equilibrium profile cannot be plotted. Hence, we define this limiting condition at which the nanofluid forms a thin film on a solid surface separating oil from the solid surface (with the spreading coefficient, $S = 0$) as the “threshold value”. Beyond the threshold value, the nanofluid spontaneously spread on the solid surface as a thin film. At the threshold value $dz/dx = 0$ and $d^2z/dx^2 = 0$ at $x = 0$, which is the axis of symmetry of the oil drop. Here, z is the meniscus height measured from the solid surface in the wedge-meniscus region and x is the radial distance measured along the solid surface from the axis of symmetry of the oil drop.

Chengara et al.’s¹⁰ equilibrium analysis is only valid when the nanofluid does not completely wet the solid surface and the spreading coefficient is negative, i.e., $S < 0$. Therefore, the spontaneous spreading of the nanofluid as a film on the solid surface cannot be inferred from their theoretical analysis.

The spontaneous spreading of an aqueous nanofluid (containing surfactant micelles) as a thin film on a hydrophilic solid surface was first observed by Kao et al.⁴⁵ in their experiments using combined differential and common light interference microscopy when the oil droplet was being removed from a glass surface. Wasan and Nikolov²⁹ recently confirmed the existence of the nanofluid aqueous film containing nanoparticles between the oil droplet and the solid; they showed that, in a wedge-shaped geometry, particles in the aqueous medium can arrange themselves in well-ordered layers.

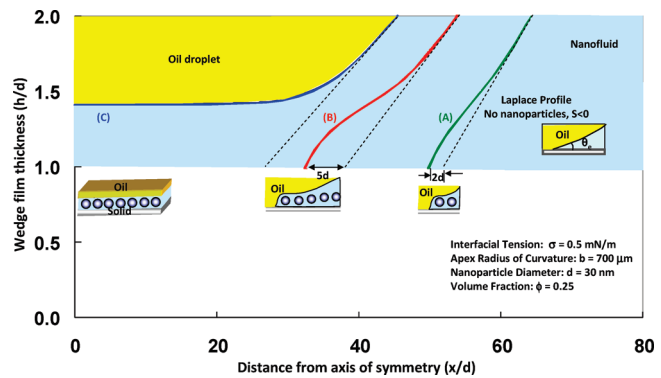


Figure 4. Effect of the contact angle on the meniscus profile in the presence of nanofluid. Solid lines are profiles with nanoparticles, dotted lines are profiles in the absence of nanoparticles: (A) $\theta_e = 4.0^\circ$, $S < 0$; (B) $\theta_e = 3.0^\circ$, $S < 0$; (C) $\theta_e = 2.3^\circ$, $S = 0$ (nanofluid film).

Technological Parameters Affecting the Spreading of a Nanofluid Film Due to the Structural Disjoining Pressure. According to Frumkin–Derjaguin (eq 3 for the spreading coefficient), the important parameters affecting the spreading of a nanofluid are the capillary and hydrostatic pressures in the bulk meniscus, the three-phase contact angle, and the film energy (which is the integral of the disjoining pressure arising due to the nanoparticle structuring in the wedge film and the contact angle at the vertex of the wedge). The contact angle greatly affects the nanoparticle structuring phenomena in the confined wedge film. Boda et al.⁴ reported that the particles are more structured (resulting in an increase in the structural disjoining pressure) in the wedge film when the contact angle at the vertex decreased.

According to Trokhymchuk et al.⁶ (eq 8), the structural disjoining pressure can be varied by manipulating the pre-experimental factors, Π_0 , Π_1 and the period of oscillation, ω . The pre-exponential factors increase with an increase in the volume fraction, ϕ , of the nanofluid, while the period of oscillation increases with an increase in the diameter, d , of the nanoparticle. Thus, the four fundamental parameters that affect the spreading of the nanofluid due to the structural disjoining pressure are the macroscopic equilibrium contact angle, nanoparticle volume fraction (concentration) of the nanofluid, particle diameter, and the total pressure (including the capillary and hydrostatic pressures).

Effect of the Contact Angle on the Meniscus Profile. The effect of the solid–nanofluid–oil three-phase contact angle on the meniscus profile in the presence of nanoparticles is shown in Figure 4. The conditions for the simulations correspond approximately to the experimental conditions employed in our present experiments. The profiles were calculated for a 25 vol\% nanofluid in contact with an oil drop with an apex radius of curvature of $700 \text{ } \mu\text{m}$ (drop volume = $0.53 \text{ } \mu\text{L}$). The oil–nanofluid interfacial tension was 0.5 mN/m , while the contact angle was varied from 4° to 2.3° ; the latter value corresponded to the threshold value at which the spreading coefficient, S , equals 0 , and the oil drop detached from the solid surface.

The effect of the contact angle on the shape of the meniscus profile was more pronounced at low contact angles. For example, when the contact angle was 4° , the position of the nominal contact line was displaced by 2 times the particle diameter, compared to the base case (which had no particles present); this can be seen in the curves (Laplace profile) when the structural disjoining pressure is zero in eq 7. However, the displacement in

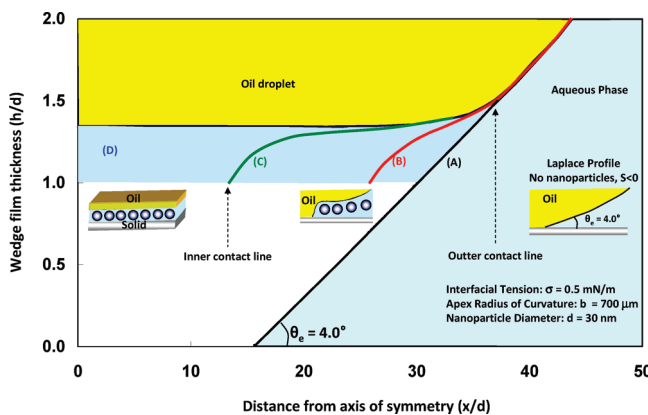


Figure 5. Effect of the nanoparticle concentration on the meniscus profile: (A) Laplace profile, no nanoparticles, $S < 0$; (B) $\phi = 30.0$ vol %, $S < 0$; (C) $\phi = 31.0$ vol %, $S < 0$; (D) $\phi = 31.4$ vol %, $S = 0$ (nanofluid film).

the nominal contact line increased to 5 times the particle diameter when the contact angle was decreased to 3° . Upon a further decrease in the contact angle to the threshold value of 2.3° , the nanofluid film formed and it separated the oil drop from the solid surface. The dependence of the three-phase contact line displacement on the contact angle was nonlinear, which is consistent with the form of eq 3 for the spreading coefficient.

It should be noted that the wedge-meniscus profiles were obtained from the equilibrium analysis. The structural disjoining pressure in the film (at $h/d = 1.4$) was balanced by the sum of the capillary pressure (i.e., from the apex radius of the drop) and the hydrostatic pressure of the drop at a contact angle of 2.3° . When the contact angle was 3° , the structural disjoining pressure (at $h/d = 1.4$) was balanced by the local capillary pressure (i.e., from the local radius of curvature).

The formation of the nanofluid film at low contact angles ($<5^\circ$) suggests that the more hydrophilic surface aids in spreading the nanofluid film on the solid surface by confining the nanoparticles in the film-meniscus region and enhancing the structural disjoining pressure. The nanofluid completely wets and spreads as a film on the solid surface, even at a finite contact angle, due to the structural disjoining pressure arising from the confinement of the nanoparticles in the wedge film.

Effect of the Nanoparticle Concentration on the Meniscus Profile. Figure 5 shows the effect of varying the nanoparticle volume concentration on the displacement of the contact line when all other parameters were held constant and the three-phase angle was 4° (measured from the aqueous phase). The extent of the displacement in the position of the nominal contact line increased with an increase in the nanoparticle volume concentration. This displacement in the nominal contact line corresponded to a bright line called the “Inner” contact line when viewed from the top using a microscope (as seen in Figure 13). The point of deviation of the wedge-film profile from the classical Laplace profile (marked in Figure 5) was seen (from the top view) as the conventional “Outer” contact line. These theoretical results predicted the experimentally observed contact lines.

As the volume concentration of nanoparticles increased, the wedge-meniscus profile resulted in the formation of a thin nanofluid film at a threshold concentration of 31.4 vol % with a spreading coefficient of $S = 0$, and it displaced the oil droplet from the solid surface. This is because as the concentration increased from 30 to 31.4 vol %, the structural disjoining pressure

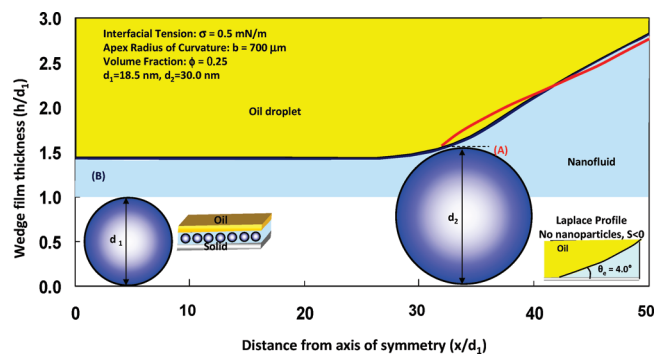


Figure 6. Effect of the nanofluid particle size on the meniscus profile: (A) $d_2 = 30$ nm, $S < 0$; (B) $d_1 = 18.5$ nm, $S = 0$ (nanofluid film).

increased from 1.1×10^5 to 1.8×10^5 dyn/cm², an increase of 63%. The nonlinear dependence of the contact line displacement on the nanoparticle volume concentration is again consistent with that given by Trokhymchuk et al.⁶ for the structural disjoining pressure (eq 8).

Effect of the Nanoparticle Size on the Meniscus Profile. The effect of the nanoparticle size (diameter) on the meniscus profile is shown in Figure 6. The nanoparticle’s diameter decreased from 30 to 18.5 nm. The computation of the meniscus profile was terminated when the height of the film became equal to one particle diameter. This means that for the 30 nm nanoparticle, the computation was terminated at a higher value of the wedge-film thickness (h); the 18.5 nm particle’s profile was computed with a lower value of h . The displacement of the nominal contact line for the 30 nm nanoparticle was not very pronounced; this is also evident in Figure 4, since all the other parameters were the same. However, when the particle size decreased to 18.5 nm, the nanofluid film formation had a spreading coefficient of $S = 0$, marking this value (i.e., 18.5 nm) as the threshold value in the particle size when the oil drop separated from the solid surface.

According to the theoretical analysis of Trokhymchuk et al.,⁶ the film disjoining pressure isotherm is a function of the particle diameter for a fixed value of the volume fraction of the nanofluid. The amplitude of oscillation in the structural film disjoining pressure (Figure 1) increases as the particle diameter decreases. For example, the structural disjoining pressure arising from the confinement of one layer of nanoparticles in the film for a 25 vol % nanofluid with a particle size of 18.5 nm is 9.5×10^4 dyn/cm² compared to 2.2×10^4 dyn/cm² for a 30 nm particle (i.e., 4.3 times higher).

The number concentration of the particles ($6\phi/\pi d^3$) in the system with 30 nm particles is 1.8×10^{16} particles/cm³, whereas for a nanofluid with 18.5 nm particles, it is 7.5×10^{16} particles/cm³. Consequently, more particles are pumped into the film by the entropic forces from a system with smaller particles. Therefore, the structural disjoining pressure is higher and the displacement of the nominal contact line is more pronounced for smaller particles in a fixed volume fraction of the nanofluid.

The advantage of using smaller particles is that the spreading of the nanofluid can occur on an even less hydrophilic surface. Figure 7 shows the particle size decreased from 18.5 to 10 nm and the three-phase contact angle was 7.9° . All other parameters were held constant. Figure 7 shows the meniscus profile for a 25 vol % nanofluid containing 10 nm particles and compares it with a 18.5 nm particle system (with a base case containing no particles). While there was very little displacement of the nanofluid containing

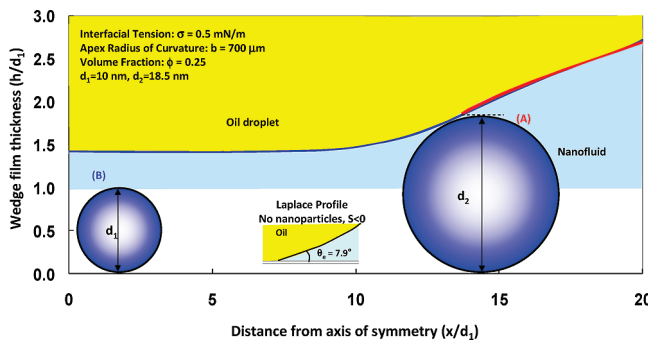


Figure 7. Effect of the nanofluid particle size on the meniscus profile: (A) $d_2 = 18.5 \text{ nm}$, $S < 0$; (B) $d_1 = 10.0 \text{ nm}$, $S = 0$ (nanofluid film).

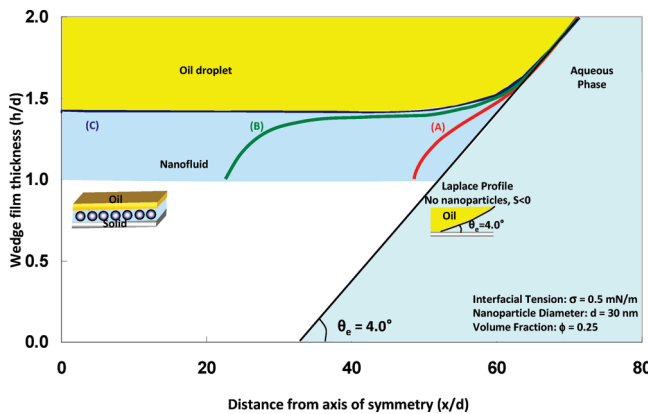


Figure 8. Effect of the drop size on the nanofluid film spreading on solid surface meniscus profile for drop size with apex radius of curvature (A) $b = 700 \mu\text{m}$, $S < 0$, (B) $b = 2200 \mu\text{m}$, $S < 0$, and (C) $b = 1.2 \text{ cm}$, $S = 0$ (nanofluid film).

18.5 nm particles compared to the base case, the system with smaller particles showed the formation of the spreading nanofluid film. This result suggests that upon decreasing the particle size from 18.5 to 10 nm, it is possible for a nanofluid to spread on a less hydrophilic surface (7.9°). The spreading of a nanofluid on a solid surface at a higher contact angle (7.9°) can be rationalized in terms of the effective axial distance over which the structural disjoining pressure acts. The effective distance is the horizontal distance along the solid surface measured from the three-phase contact line until the point where the meniscus height corresponds to one particle diameter of the nanofluid. If we assume that the wedge region in the absence of nanoparticles (base case) with a 15° contact angle is nondeformable, then the effective distance for an 18.5 nm particle system is about 60 nm; it is 37 nm for a 10 nm nanofluid. The magnitude of the structural force at one particle diameter was estimated using eq 8 to be $9.5 \times 10^4 \text{ dyn/cm}^2$ for the 18.5 nm nanofluid and $6 \times 10^5 \text{ dyn/cm}^2$ for a 10 nm nanofluid. Thus, the gradient of the structural disjoining pressure driving the spreading of the nanofluid in the film region in the 10 nm system is an order of magnitude higher than in the 18.5 nm system. The spreading of a nanofluid on a solid surface at a higher contact angle can be facilitated if we use smaller nanoparticles and higher volume concentrations of the nanofluid.

Effect of the Capillary Pressure on the Meniscus Profile. Equation 3 shows that the spreading due to the structural disjoining pressure (or film tension) gradient is resisted by the capillary and hydrostatic pressures inside the oil drop. So for the

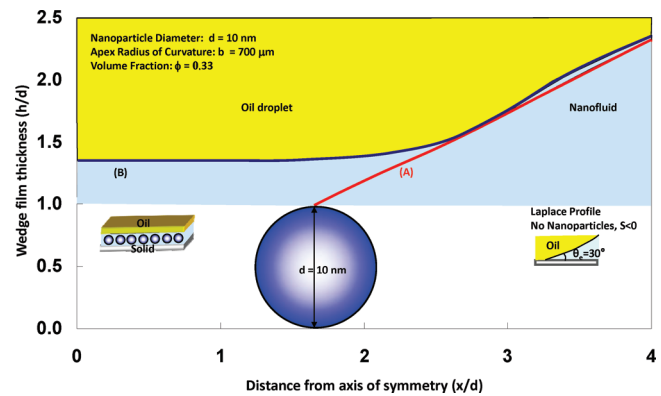


Figure 9. Effect of the interfacial tension on the nanofluid film spreading on solid surface: (A) $\sigma = 0.5 \text{ mN/m}$, $S < 0$; (B) $\sigma = 0.1 \text{ mN/m}$, $S = 0$ (nanofluid film).

same spreading force (structural disjoining pressure), we expect less displacement of the contact line when the total pressure (i.e., capillary and hydrostatic pressure) is higher. The total pressure of the drop depends on the drop size and the interfacial tension. The effect on the displacement of the contact line of varying only the drop size while keeping the interfacial tension constant at 0.5 mN/m is illustrated in Figure 8. This figure shows that as the drop size decreased from 10.8 to 0.53 μL (i.e., the radius of curvature from 1.2 cm to 700 μm), the displacement in the position of the nominal contact line also decreased. This is because the total pressure increased from 22.2 to 29.2 dyn/cm^2 as the drop size decreased. The nanofluid spread spontaneously ($S = 0$) as a thin film for a 10.8 μL drop, which is the threshold value. However, spreading was not seen for a drop size of 0.53 μL .

The effect of varying only the interfacial tension on the displacement of the contact line while keeping the drop size constant (i.e., apex radius of curvature) is seen in Figure 9. It should be noted that the nanofluid can spread as a thin film on a solid surface (i.e., $S = 0$) due to the lowering of the interfacial tension from 0.5 to 0.1 mN/m, even at a higher contact angle of 30° . The nanofluid volume concentration is 33 vol %, and the particle size is 10 nm. This is because when the interfacial tension decreased from 0.5 to 0.1 mN/m, the total resisting force for the spreading of the nanofluid decreased from 28.8 to 13.0 dyn/cm^2 .

In summary, we are reporting, for the first time, that the spreading of a nanofluid as a film on a solid surface is possible even at higher contact angles ($\sim 20^\circ$) by decreasing the particle size to 10 nm and by decreasing the interfacial tension to 0.1 mN/m. Furthermore, our systematic parametric studies based on statics analysis clearly show that when the interfacial tension is 0.5 mN/m, both the low equilibrium three-phase contact angle ($\leq 5^\circ$) and high concentration of the nanofluid ($> 25 \text{ vol } \%$) are desirable parameters for the spreading of the nanofluid as a film on a solid surface.

Surface Plot of the Threshold Values for the Important Parameters of Spreading. Figures 4–9 show the results of the parametric study for the displacement of the three-phase contact line and the spontaneous spreading of the nanofluid as a film on the solid surface due to the structural disjoining pressure gradient (arising from the confinement of the nanoparticles in the wedge film). Table 1 lists all the parameters for the calculations presented in these plots. This table indicates that when the particle size is held constant and the interfacial tension is fixed at

Table 1. List of Parameters Affecting Spreading of Nanofluid and the Corresponding Value of Structural Disjoining Pressure at One-Layer Thick Film Containing Nanoparticles

figure no.	contact angle (θ_e , deg)	effective volume (ϕ_e , %)	effective Diameter (d _e , nm)	interfacial tension σ , dyn/cm	apex curvature (b, μm) and drop volume (μL)	capillary pressure + hydrostatic pressure = total pressure (dyn/cm ²)	structural disjoining pressure at film thickness corresponding to one layer of nanoparticles (dyn/cm ²)
3	1.0	25.4	20.0	20.0	500 μm (0.52 μL)	800 + 19.1 = 819.1	84 800
3	1.0	25.0	20.0	20.0	500 μm (0.52 μL)	800 + 19.1 = 819.1	75 291
4	2.3	25.0	30.0	0.5	700 μm (0.53 μL)	14.4 + 15.0 = 29.4	22 308
4	3.0	25.0	30.0	0.5	700 μm (0.53 μL)	14.4 + 15.0 = 29.4	22 308
4	4.0	25.0	30.0	0.5	700 μm (0.53 μL)	14.4 + 15.0 = 29.4	22 308
4	5.0	25.0	30.0	0.5	700 μm (0.53 μL)	14.4 + 15.0 = 29.4	22 308
5	4.0	30.0	30.0	0.5	700 μm (0.53 μL)	14.4 + 15.0 = 29.4	110 512
5	4.0	31.4	30.0	0.5	700 μm (0.53 μL)	14.4 + 15.0 = 29.4	182 905
6	4.0	25.0	18.5	0.5	700 μm (0.53 μL)	14.4 + 15.0 = 29.4	95 130
6	4.0	25.0	30.0	0.5	700 μm (0.53 μL)	14.4 + 15.0 = 29.4	22 308
7	15.0	35.0	18.5	0.5	700 μm (0.528 μL)	14.4 + 14.8 = 29.2	3 332 604
7	15.0	35.0	10.0	0.5	700 μm (0.528 μL)	14.4 + 14.8 = 29.2	21 100 798
8	4.0	25.0	30.0	0.5	700 μm (0.53 μL)	14.4 + 14.8 = 29.2	22 308
8	4.0	25.0	30.0	0.5	2200 μm (2.78 μL)	4.6 + 19.5 = 24.1	22 308
8	4.0	25.0	30.0	0.5	1.2 cm (10.8 μL)	0.8 + 21.4 = 22.2	22 308
9	30.0	33.0	10.0	0.5	700 μm (0.517 μL)	14.4 + 14.4 = 28.8	9 133 745
9	30.0	33.0	10.0	0.1	700 μm (0.05 μL)	6.5 + 6.4 = 12.9	9 133 745
10	1.0	19.1	30.0	0.5	700 μm (0.53 μL)	14.4 + 15.0 = 29.4	4292
10	1.0	21.2	30.0	0.5	2200 μm (2.78 μL)	4.6 + 19.5 = 24.1	7589
10	1.0	19.0	30.0	0.5	4380 μm (5.32 μL)	2.3 + 20.7 = 23.0	4178
10	1.0	17.8	30.0	0.5	7000 μm (7.52 μL)	1.4 + 21.1 = 22.5	3027
10	3.0	27.2	30.0	0.5	700 μm (0.53 μL)	14.4 + 15.0 = 29.4	43 658
10	3.0	27.4	30.0	0.5	2200 μm (2.78 μL)	4.6 + 19.5 = 24.1	46 512
10	3.0	27.3	30.0	0.5	4380 μm (5.32 μL)	2.3 + 20.7 = 23.0	45 060
10	3.0	28.4	30.0	0.5	7000 μm (7.52 μL)	1.4 + 21.1 = 22.5	64 255
10	5.0	34.6	30.0	0.5	700 μm (0.53 μL)	14.4 + 15.0 = 29.4	656 579
10	5.0	34.4	30.0	0.5	2200 μm (2.78 μL)	4.6 + 19.5 = 24.1	602 606
10	5.0	34.9	30.0	0.5	4380 μm (5.32 μL)	2.3 + 20.7 = 23.0	747 960
10	5.0	35.4	30.0	0.5	7000 μm (7.52 μL)	1.4 + 21.1 = 22.5	933 575
11	0.5	6.4	10.0	0.5	7000 μm (7.52 μL)	1.4 + 21.1 = 22.5	2437
11	0.5	13.9	20.0	0.5	4380 μm (5.32 μL)	2.3 + 20.7 = 23.0	3540
11	0.5	19.8	30.0	0.5	2200 μm (2.78 μL)	4.6 + 19.5 = 24.1	5184
11	0.5	24.8	43.0	0.5	700 μm (0.53 μL)	14.4 + 15.0 = 29.4	7142
11	1.0	7.6	10.0	0.5	7000 μm (7.52 μL)	1.4 + 21.1 = 22.5	3919
11	1.0	15.4	20.0	0.5	4380 μm (5.32 μL)	2.3 + 20.7 = 23.0	5350
11	1.0	21.6	30.0	0.5	2200 μm (2.78 μL)	4.6 + 19.5 = 24.1	8471
11	1.0	26.9	43.0	0.5	700 μm (0.53 μL)	14.4 + 15.0 = 29.4	13 493
11	2.0	9.9	10.0	0.5	7000 μm (7.52 μL)	1.4 + 21.1 = 22.5	8661
11	2.0	18.4	20.0	0.5	4380 μm (5.32 μL)	2.3 + 20.7 = 23.0	12 003
11	2.0	25.1	30.0	0.5	2200 μm (2.78 μL)	4.6 + 19.5 = 24.1	22 979
11	2.0	31.1	43.0	0.5	700 μm (0.53 μL)	14.4 + 15.0 = 29.4	55 616
11	3.0	12.2	10.0	0.5	7000 μm (7.52 μL)	1.4 + 21.1 = 22.5	17 456
11	3.0	21.5	20.0	0.5	4380 μm (5.32 μL)	2.3 + 20.7 = 23.0	27 813
11	3.0	28.6	30.0	0.5	2200 μm (2.78 μL)	4.6 + 19.5 = 24.1	68 640
11	3.0	35.4	43.0	0.5	700 μm (0.53 μL)	14.4 + 15.0 = 29.4	317 035
11	4.0	14.5	10.0	0.5	7000 μm (7.52 μL)	1.4 + 21.1 = 22.5	33 447
11	4.0	24.5	20.0	0.5	4380 μm (5.32 μL)	2.3 + 20.7 = 23.0	65 002
11	4.0	32.1	30.0	0.5	2200 μm (2.78 μL)	4.6 + 19.5 = 24.1	238 058
11	4.0	39.7	43.0	0.5	700 μm (0.53 μL)	14.4 + 15.0 = 29.4	2 794 656

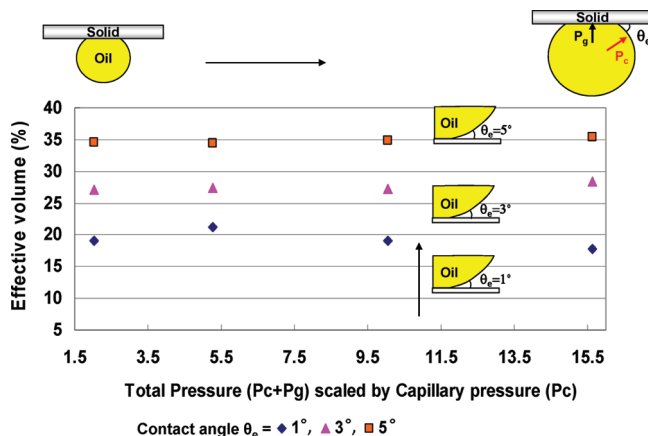


Figure 10. Threshold volume fraction for spreading of 30 nm nanofluid for different drop sizes at a fixed equilibrium three phase contact angle (θ_e).

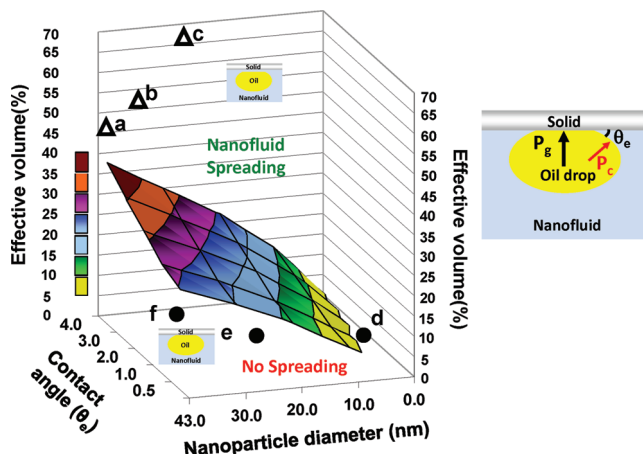


Figure 11. Surface plot of threshold values of parameters resulting in spreading of nanofluid with the experimental data points.

0.5 mN/m, the threshold values (when $S = 0$) of the nanofluid concentration (effective volume) required for it to spread as a thin film do not vary as much the drop radius of curvature at its apex (i.e., as the oil drop sizes (or capillary pressure and hydrostatic pressure) are varied). An example of this is illustrated in Figure 10 for a 30 nm particle nanofluid system with a low contact angle ($\leq 5^\circ$).

Figure 11 shows a three-dimensional surface plot depicting the threshold values of the various parameters for the spreading of the nanofluid. Since the spreading coefficient does not vary much with the total pressure of the drop for the nanofluid–oil system studied here, its dependence on the total pressure is not shown on this plot. This figure depicts the spreading dependency on the contact angle, nanofluid concentration (volume fraction), and particle size. Our analysis is based on the assumption that nanoparticles are hard-sphere particles. To compare the theoretical results with experimental results, if the nanoparticles are charged, one can assume that they would act as hard spheres with a particle size equal to the effective diameter of the nanoparticles (the sum of the nominal diameter and double layer thickness). This assumption is reasonable as experiments showed that the film thickness with one layer of particles corresponds to the effective diameter of the nanoparticles.¹⁸ The surface plot shows

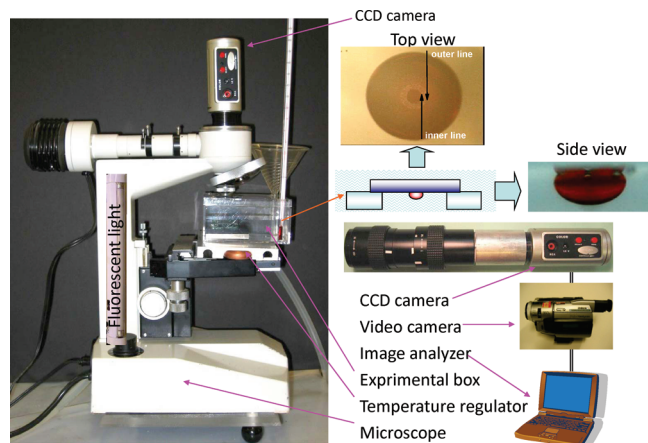


Figure 12. Apparatus and experimental setup for monitoring nanofluid spreading dynamics and micrographs depicting the top and side views of the drop.

that a combination of parameters can result not only in the displacement of the three-phase contact line but also in the spreading of the nanofluid as a film. The foremost prediction from our statics analysis is that a suitable combination of the nanofluid concentration, particle size, and contact angle (which lies above or on the surface plot) would result in the spontaneous spreading of the nanofluid as a film on the solid substrate.

We have conducted some preliminary experiments on the spreading dynamics of a nanofluid composed of a silica suspension of nanoparticles in water and a drop of canola oil placed on a glass surface. Our experimental data points (some of which lie above and others below the surface plot) validating the theoretical analysis are also shown in Figure 11. These experiments are summarized below.

EXPERIMENTS

The major finding of our theoretical analysis (which takes into account the contribution of the structural disjoining pressure) is that the spreading of the nanofluid as a film over the solid greatly depends on the concentration of nanoparticles, their size and the film-meniscus contact angle. We found that the displacement of the nominal contact line is greater when the concentration (effective volume) is large, the nanoparticle diameter is small (at a fixed particle volume concentration), and the contact angle is small ($\leq 5^\circ$), as shown in Figure 3. We have conducted experimental observations of the spreading of the nanofluids driven by the structural disjoining pressure gradient to validate our theoretical analysis. These experiments are described below.

Figure 12 shows the layout of the apparatus used to perform the experiments. An oil drop of a specific volume was deposited from a syringe under the lower surface of a hydrophilic, optically smooth glass surface, which was then immersed in the nanofluid in an experimental box with a controlled environment. Two square glass supports were used to lift the glass slide to provide good visual observation. The dynamics of nanofluid spreading on the solid surface were simultaneously monitored and recorded by two sets of digital CCD video cameras from the top and side views at 30 frames per second. The video images were digitized by image analyzer software (Image-Pro Plus) for further analysis. Two distinct lines (the inner and outer lines, Figure 12) were observed during the nanofluid spreading. The positions of the inner and outer contact lines were monitored in the top view via a vertical microscope in reflected light mode with a long focus objective. The side view was captured by a horizontal microscope in transmitted light mode with a

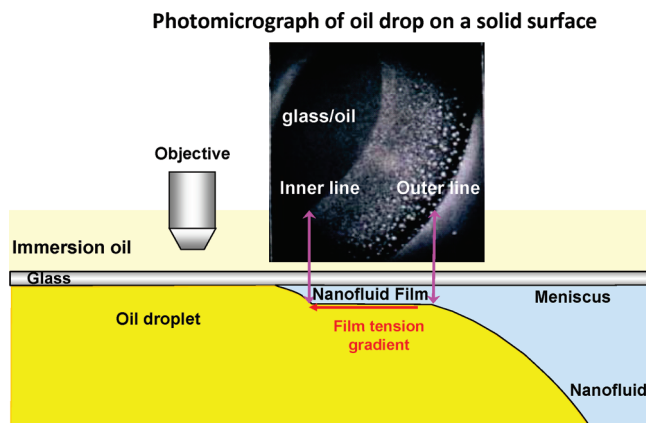


Figure 13. Photomicrograph taken using reflected light interferometry depicting the inner and outer contact lines and the nanofluid film region.

high magnification lens. The side-view lens was adjusted so that the droplet reflection on the glass and the position of the outer contact line were always observed. The drop profile was recorded in the side view and drop shape analysis was used to calculate the interfacial tension between the oil phase and the nanofluid. The drop profile obtained using a goniometer (Kernco Instruments, Inc.) was fitted with the Laplace equation, and the interfacial tension thus obtained was found comparable with the interfacial tension obtained using our experimental setup. The accuracy in the measurement of the interfacial tension is about 10%. We conducted experiments on the spreading of a nanofluid composed of 5, 10, 12.5, and 20 vol % silica suspensions of 20 nm geometric diameter particles containing 3–6 mM SDS (sodium dodecyl sulfate, much less than the critical micelle concentration, CMC) in water. SDS was used below the CMC to reduce the contact angle to enhance the confinement of nanoparticles in the wedge-film region. A drop of canola oil was placed underneath the glass surface and the spreading of the nanofluid at a pH of 9.0 and at 25 °C was investigated with our experimental apparatus. When the air was displaced by the nanofluid, the three-phase contact line shrank (due to the imbalance in the surface tension forces) until a new balance in the surface forces at the three-phase contact line was established. The nanoparticles then formed ordered structures inside the wedge and the structural disjoining pressure gradient drove the nanofluid inside the wedge region. The nanofluid containing hydrophilic particles penetrated between the oil and the glass surface, and a film was formed. The microscopic photograph depicting the inner and outer contact lines is shown in Figure 13. The outer line between the oil drop, solid surface, and the aqueous nanoparticle film is the boundary between the meniscus and the nanofilm; the inner line between the oil drop, solid surface, and the aqueous film is the boundary between the nanofilm and the oil–glass interface. Over time, the inner contact line advances and the formation of the nanofluid film is seen as a bright region in the reflected light interferometry (Figure 13). The nanofluid is considered to have completely spread ($S = 0$) when the solid–oil contact area is replaced by the bright aqueous film of the nanofluid.

We also explored the effect of an electrolyte, such as sodium chloride, on the nanofluid spreading phenomena. In our previous experiments using an anionic micellar surfactant solution (0.1 M SDS), we noticed that the oil droplet shrank due to the reduction in the interfacial tension between the oil and the aqueous micellar solution at a higher salt concentration (0.1 M NaCl), but the formation of the nanofluid film was not seen in this case²⁹ and the nanofluid did not spread over the solid surface. At a high salt concentration, the effective micellar diameter (and thereby the micellar volume fraction) decreases because of the shrinkage of the electrical double layers around each micelle. The magnitude of the structural disjoining pressure diminishes, reducing the driving force for spreading.

Table 2. Properties of Nanofluid

manufacturer	Johnson Matthey Electronics		
nanoparticle type	silicon(iv) oxide		
pH	9.0		
viscosity	25 cps at 20 V%		
density	1.30		
nominal diameter/geometric	20 nm		
polydispersity	N/A		
nanofluid concentration (nominal volume, ϕ , vol %)	NaCl salt concentration added	effective volume (ϕ_e), vol %	effective diameter (nm)
20		66	30
12.5		50	38
10		45	43
5	2.6 mM	~9.5	30
5	0.1 M	~3	21

The properties of the nanofluid and its various formulations used in our experiments are listed in Table 2. The results of the experiments are summarized in Table 3 and plotted in Figure 11. The effective size of the nanoparticles (d_e , including the electrical double layer) and thereby the effective volume of the nanofluid formulation (ϕ_e), was determined using our capillary force balance apparatus in conjunction with the reflected light common interferometric technique.^{18–21} The contact angle was obtained by fitting the Laplace equation to the drop shape profile for a fixed contact radius measured in the top view.

The experimental results demonstrate that the effective particle size of about 40 nm, a low contact angle ($\theta_e < 3^\circ$), and the effective concentration of the nanofluid >30 vol % are desirable for the dynamic spreading of nanofluid as a film on the solid surface. Figure 11 shows that the experimental data points that lie above (a–c) and also below (d–f) the surface plot validate the prediction from the statics analysis.

CONCLUDING REMARKS

We have reported here the results of our experimental and theoretical studies on the spontaneous spreading of a nanofluid as a film over a solid surface under the action of the structural disjoining pressure. The structural disjoining pressure acts normal to the solid–liquid interface and arises due to the nanoparticle structuring in the wedge film formed between an oil drop and a solid surface. Our theoretical analysis extends the previous statics analysis of Chengara et al.^{10,30} for the wedge profile by predicting the threshold values of important technological factors such as the nanofluid concentration, particle size, contact angle, and capillary pressure at which the nanofluid spreads as a film ($S = 0$) and completely wets the solid surface. The results of the computations are presented in a three-dimensional surface plot depicting the dependency of spreading on the threshold values of the various parameters (Figure 11). The threshold values were found to be strong functions of the nanofluid concentration, particle size, and the three-phase contact angle, but a weak function of the capillary pressure (drop size) for the oil–nanofluid system with an interfacial tension of 0.5 mN/m investigated here. Our experimental data for the oil–nanofluid of aqueous suspensions of 5, 10, 12.5, and 20 vol % (nominal volume) (and a low contact angle of <3°) are also shown on this plot (Figure 11). These data seem to validate the foremost prediction of our theoretical analysis.

According to the classical theory of wetting, pure liquids (without any particles) completely wet the surface only when

Table 3. Experimental Observations of Spreading (or No Spreading) for Various Concentrations of Nanofluid

	nanofluid nominal volume (ϕ)	nanofluid Effective volume (ϕ_e)	SDS added, mM	NaCl salt added	effective diameter (d_e , nm)	contact angle (θ_e , deg)	film energy (J/m ²)	experimental observation
a	10v%	45v%	3		43	1.9	-2.2×10^{-6}	spreading
b	12.5v%	50v%	6		38	3.0	-4.3×10^{-6}	spreading
c	20v%	66v%	3		30	2.6	-2.0×10^{-5}	spreading
d	pH 9 water	0v%	6	0.185 M	0	3.0	0.0	no spreading
e	5v%	~3v%	3	0.1 M	21	1.6	-4.1×10^{-9}	no spreading
f	5v%	~9.5v%	3	2.6 mM	30	2.1	-1.4×10^{-8}	no spreading
	12.5v%	50v%	3		38	6.2	-4.3×10^{-9}	no spreading

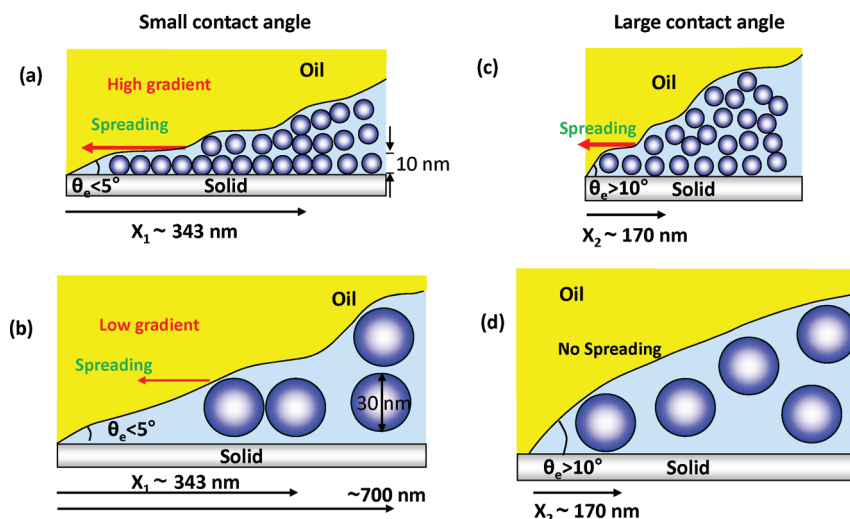


Figure 14. (a) and (b) Schematic showing multilayering of small particles at small contact angles while large particles form only one layer for the same axial distance X_1 . (c) and (d) Schematic shows that axial distance for large contact angle $X_2 < X_1$. Small particles form layered structure over short distance due to size effect and result in nanofluid spreading. Large particles cannot form ordered structures in such short distance X_2 when confinement is wide. So no spreading of nanofluid.

the contact angle is zero. A major finding of our present theoretical analysis is that the complete wetting and spontaneous spreading of the nanofluid (driven by the structural disjoining pressure gradient) as a film on a solid surface is possible, even at higher values of the contact angle, by manipulating the nanofluid concentration, nanoparticle size, and interfacial tension. However, an experimental study needs to be conducted in the future using systems with higher contact angles to corroborate our theoretical findings.

Figure 14 depicts the two-dimensional ordering of the small and large particles at the same volume fraction in the wedge confinement at both small and large contact angles. For a small contact angle ($\leq 5^\circ$), the small particles tend to form multiple layers (Figure 14a), whereas large particles form a single layer (Figure 14b) over the same axial distance, X_1 , over which the structural disjoining pressure acts. The axial distance along the solid surface is measured from the vertex until the point where the meniscus height corresponds to one large particle diameter of the nanofluid.

Since the structural disjoining pressure (or film tension) is higher near the vertex, the structural pressure gradient over the length of the wedge drives the nanofluid to spread out (i.e., the three-phase contact line moves). Also, the structural pressure gradient is lower for large particles, so the displacement of the three-phase contact line is less (Figure 6).

Parts c and d of Figure 14 depict the particle layering phenomenon of the small and large size particles in the confined region of the wedge film at a high contact angle ($>10^\circ$), respectively. Since the contact angle is large, the axial distance, X_2 , is smaller than X_1 and the structural disjoining pressure acts over a shorter distance. Also, even at a high contact angle, the small particles with a higher number density (at a fixed particle volume concentration) form a better layered structure (Figure 14c) than the larger particles (Figure 14d), resulting in a significant pressure gradient to spread the nanofluid as a film on a solid surface. Therefore, the spreading of the nanofluid on a less hydrophilic surface is achievable by decreasing the size of the particles and increasing their concentration. The large particles cannot form any ordered structures at large contact angles (Figure 14d) as the confinement is too wide, making spreading impossible.

Our computations for determining the wedge-film profile and the displacement of the three-phase contact line are based on the structural disjoining pressure (or film energy) gradient and the no-slip boundary condition. Therefore, the van der Waals and electrostatic contributions to the film energy given by the conventional DLVO theory were not considered.

We used the analytical expression for the structural disjoining pressure isotherm given by Trokhymchuk et al.,⁶ which is valid when the nanoparticles (as hard spheres) are confined in a

vacuum in a film bounded by two parallel, rigid solid surfaces; therefore, it is valid for a symmetric film. However, our nanoparticles were suspended in a solvent confined in a film (aqueous medium) formed between a solid surface and an oil drop. The film confinement is wedge-shaped, asymmetric, and deformable. The wedge-film thickness varies along the radial distance. Therefore, to calculate the meniscus profile, the structural disjoining pressure was evaluated using the analytical expression (eq 8) given by Trokhymchuk et al.⁶ and by assuming an infinitesimal plane parallel film. We calculated the structural film energy (and thereby, the structural disjoining pressure) from the film-meniscus contact angle data measured using differential interferometry¹⁸ and found that the values of the structural disjoining pressure for an asymmetric film are somewhat lower than those calculated using the analytical expression for a symmetric film developed by Trokhymchuk et al.⁶ This suggests that the threshold values of the various parameters for the spread of the nanofluid were somewhat underestimated in the present study.

The polydispersity in the particle size affects the magnitude of the structural disjoining pressure.^{46,47} The structural disjoining pressure decreases with an increase in the polydispersity of the nanoparticle dispersion (e.g., the structural disjoining pressure decreased by half when the polydispersity increased from zero to 20%), so this effect needs to be considered when calculating the threshold values of the parameters for the spreading of polydisperse nanofluids, since most of the practical systems are polydisperse.

The charge on the particle also affects the magnitude of the structural disjoining pressure and spreading behavior. Therefore, we based our calculations of the threshold values of the spreading parameters on the effective particle diameter (including the double layer around the particle), which are shown in the surface plot (Figure 11). We assumed the nanoparticles (including double layers) were hard spheres. This assumption is reasonable since the effective thickness of the nanofluid film with one layer of particles was found experimentally to be equal to the effective diameter of the particle.¹⁸ This allows us to compare our experimental results for nanofluid spreading on the solid surface with the theoretical predictions, which is shown in the surface plot in Figure 11.

Our experiments on the spreading of nanofluids on a glass surface were performed for an oil–nanofluid system with a low contact angle (<3°) and an interfacial tension of 0.5 mN/m. A more systematic experimental study needs to be undertaken to examine the effects of various parameters, including solid substrates other than the hydrophilic glass to confine the nanoparticles and enhance the structural disjoining pressure in the wedge film. The choice of the systems to be used in future experiments will be largely guided by the theoretical predictions on spreading (Figure 11).

Finally, spreading is a dynamic process. Though the spontaneous detachment of oil drops from a solid surface in the presence of surfactant solutions has been investigated recently,^{48,49} both theoretical and experimental studies are warranted to advance the fundamental understanding of the dynamics of nanofluids (containing particles) spreading on solid surfaces. Such an effort is already underway in our laboratory, and the results will be presented in our forthcoming paper (in progress), which deals with modeling nanofluid-spreading dynamics.

AUTHOR INFORMATION

Corresponding Author

*E-mail: wasan@iit.edu.

ACKNOWLEDGMENT

This work was supported by the National Science Foundation under grant CTS-0553738.

REFERENCES

- (1) Wong, K. V.; Leon, D. O. *Adv. Mech. Eng.* **2010**, 2010, 11.
- (2) Brauman, J. I.; Szuromi, P. *Science* **1996**, 273, 855.
- (3) Nikolov, A. D.; Wasan, D. T. *Langmuir* **1992**, 8, 2985.
- (4) Boda, D.; Chan, K.-Y.; Henderson, D.; Wasan, D. T.; Nikolov, A. D. *Langmuir* **1999**, 15 (13), 4311–4313.
- (5) Tata, B. V. R.; Boda, D.; Henderson, D.; Nikolov, A.; Wasan, D. T. *Phys. Rev. E* **2000**, 62, 3875–3881.
- (6) Trokhymchuk, A.; Henderson, D.; Nikolov, A. D.; Wasan, D. T. *Langmuir* **2001**, 17, 4940–4947.
- (7) Wasan, D. T. Nikolov, A. D. Structural Transitions in Colloidal Suspensions in Confined Films. In *Supramolecular Structure in Confined Geometries*; Manne, S., Warr, G., Eds.; ACS Symposium Series No. 736; American Chemical Society: Washington, DC, 1999.
- (8) Trokhymchuk, A.; Henderson, D.; Nikolov, A.; Wasan, D. T. *Langmuir* **2005**, 21 (22), 10240–10250.
- (9) Henderson, D. J., Nikolov, A. D., Trokhymchuk, A., Wasan, D. T. Confinement-Induced Structural Forces in Colloidal Systems. In *Encyclopedia of Surface and Colloid Science*, 2nd ed.; Somasundaran, P., Ed.; Taylor and Francis: New York, 2006.
- (10) Chengara, A.; Nikolov, A. D.; Wasan, D. T.; Trokhymchuk, A.; Henderson, D. J. *Colloid Interface Sci.* **2004**, 280, 192–201.
- (11) Trokhymchuk, A.; Henderson, D.; Nikolov, A. D.; Wasan, D. T. *J. Phys. Chem. B* **2003**, 107, 3927–3937.
- (12) Trokhymchuk, A.; Henderson, D.; Nikolov, A.; Wasan, D. *Langmuir* **2004**, 20 (17), 7036–7044.
- (13) Trokhymchuk, A.; Henderson, D.; Nikolov, A.; Wasan, D. *Ind. Eng. Chem. Res.* **2005**, 44 (5), 1175–1180.
- (14) Vettiger, P.; Binning, G. *Sci. Am.* **2003**, 288, 46.
- (15) Chu, X. L.; Nikolov, A. D.; Wasan, D. T. *J. Chem. Phys.* **1995**, 103, 6653.
- (16) Wasan, D. T.; Nikolov, A.; Trokhymchuk, A.; Henderson, D. *Condens. Matter Phys.* **2001**, 4, 361.
- (17) Basheva, E. S.; Kralchevsky, P. A.; Danov, K. D.; Ananthapadmanabhan, P.; Lips, A. *Phys. Chem. Chem. Phys.* **2007**, 9, 5183.
- (18) Nikolov, A. D.; Kondiparty, K.; Wasan, D. T. *Langmuir* **2010**, 26 (11), 7665.
- (19) Nikolov, A. D.; Dimitrov, A. S.; Kralchevsky, P. A. *Opt. Acta* **1986**, 33, 1359.
- (20) Dimitrov, A. S.; Kralchevsky, P. A.; Nikolov, A. D.; Wasan, D. T. *Colloids Surf.* **1990**, 47, 299.
- (21) Nikolov, A. D. Wasan, D. T. In *Handbook of Surface Imaging and Visualization*; Hubbard, A. T., Ed.; CRC Press: New York, 1995; pp 209–214.
- (22) Chaudhury, M. K. *Nature* **2003**, 423, 131–132.
- (23) de Gennes, P. G. *Rev. Mod. Phys.* **1985**, 57, 827–863.
- (24) Churaev, N. V. *Colloids Surf. A* **1993**, 79, 25–31.
- (25) Ruckenstein, E. J. *Colloid Interface Sci.* **1996**, 179, 136–142.
- (26) Churaev, N. V.; Esipova, N. E.; Hill, R. M.; Sobolev, V. D.; Starov, V. M.; Zorin, Z. M. *Langmuir* **2001**, 17, 1338–1348.
- (27) De Coninck, J.; de Ruijter, M. J.; Voué, M. *Curr. Opin. Colloid Interface Sci.* **2001**, 6, 49–53.
- (28) Cazabat, A. M.; Fraysse, N.; Heslot, F. *Colloids Surf.* **1991**, 52, 1–8.
- (29) Wasan, D. T.; Nikolov, A. D. *Nature* **2003**, 423, 156.
- (30) Chengara, A. V.; Nikolov, A. D.; Wasan, D. T. *Adv. Polym. Sci.* **2008**, 218, 117.

- (31) Matar, O. K.; Craster, R. V.; Sefiane, K. *Phys. Rev. E* **2007**, *76*, 056315.
- (32) Sefiane, K.; Skilling, J.; MacGillivray, J. *Adv. Colloid Interface Sci.* **2008**, *138*, 101.
- (33) Craster, R. V.; Matar, O. K.; Sefiane, K. *Langmuir* **2009**, *25*, 3601.
- (34) Moffat, J. R.; Sefiane, K.; Bennacer, K.; Guo, Y. Recent Progress on Nanofluids and Their Potential Applications. In *Nanoscience: Colloidal And Interfacial Aspects*; Starov, V., Ed.; Surfactant Science Series; Taylor and Francis/CRC Press: Boca Raton, FL, 2010; Vol. 147.
- (35) de Gennes, P. G. *Rev. Mod. Phys.* **1985**, *57*, 827.
- (36) Derjaguin, B. V. In *Theory of Stability of Colloids and Thin Films*; Johnson, R. K., Ed.; Consultants Bureau: New York, 1989.
- (37) Churaev, N. V. In *Liquid and Vapor Flows in Porous Bodies: Surface Phenomena*; Galwey, A., Ed.; Overseas Publishers Association: Amsterdam, 2000.
- (38) Churaev, N. V.; Zorin, Z. M. *Adv. Colloid Interface Sci.* **1992**, *40*, 109.
- (39) Churaev, N. V. *Adv. Colloid Interface Sci.* **2003**, *103*, 197.
- (40) Hirasaki, G. J. *SPE Form. Eval.* **1991**, No. June, 217.
- (41) Churaev, N. V. *Adv. Colloid Interface Sci.* **2003**, *104*, xv–xx.
- (42) Starov, V. M. *Adv. Colloid Interface Sci.* **1992**, *39*, 147.
- (43) Bangham, D. H.; Razouk, R. I. *Trans. Faraday Soc.* **1937**, *33*, 1459.
- (44) Starov, V. M.; Velarde, M. G. *J. Phys.: Condens. Matter* **2009**, *21*, 464121.
- (45) Kao, R. L.; Wasan, D. T.; Nikolov, A. D.; Edwards, D. A. *Colloids Surf. A* **1988**, *34*, 389–398.
- (46) Piech, M.; Walz, J. Y. *J. Colloid Interface Sci.* **2002**, *253*, 117–129.
- (47) Chu, X. L.; Nikolov, A. D.; Wasan, D. T. *Langmuir* **1996**, *12* (21), 5004–5010.
- (48) Kolev, V. L.; Kochijashky, I. I.; Danov, K. D.; Kralchevsky, P. A.; Broze, G.; Mehreteab, A. J. *Colloid Interface Sci.* **2003**, *257*, 357.
- (49) Kralchevsky, P. A.; Danov, K. D.; Kolev, V. L.; Gurkov, T. D.; Temelska, M. I.; Brenn, G. *Ind. Eng. Chem. Res.* **2005**, *44*, 1309.
- (50) Hirasaki, G. J. In *Interfacial Phenomena in Petroleum Recovery*; Morrow, N. R., Ed.; Marcel Dekker: New York, 1991; Chapter 2.
- (51) Zhang, X.; Neogi, P.; Ybarra, R. M. *J. Colloid Interface Sci.* **2002**, *249*, 134–140.
- (52) Starov, V. M. *Adv. Colloid Interface Sci.* **1992**, *39*, 147.
- (53) Brochard-Wyart, F.; di Meglio, J. M.; Quéré, D.; de Gennes, P. G. *Langmuir* **1991**, *7*, 335.
- (54) Yeh, E. K.; Newman, J.; Radke, C. J. *Colloid Surfaces A* **1999**, *156*, 525.
- (55) Wayner, P. C., Jr. *J. Colloid Interface Sci.* **1980**, *77*, 495.
- (56) Truong, J. G.; Wayner, P. C., Jr. *J. Chem. Phys.* **1987**, *87*, 4180.
- (57) Frumkin, A. N. *Zh. Fiz. Khim.* **1938**, *12* (4), 337.
- (58) Derjaguin, B. V. *Zh. Fiz. Khim.* **1940**, *14* (2), 137.
- (59) Shanahan, E. R. *Langmuir* **2001**, *17* (13), 3997–4002. Shanahan, E. R. *Langmuir* **2001**, *17* (26), 8229–8235.